Wavefront Tilt Feedforward for the Formation Interferometer Testbed (FIT)

Joel Shields *[a], Kurt Liewer [a], Udo Wehmeier [a]
[a] Jet Propulsion Laboratory, California Institute of Technology

ABSTRACT

Separated spacecraft interferometry is a candidate architecture for several future NASA missions. The Formation Interferometer Testbed (FIT) is a ground based testbed dedicated to the validation of this key technology for a formation of two spacecraft. In separated spacecraft interferometry,th e residual relative motion of the component spacecraft must be compensated for by articulation of the optical components.

In this paper, the design of the FIT interferometer pointing control system is described. This control system is composed of a metrology pointing loop that maintains an optical link between the two spacecraft and two stellar pointing loops for stabilizing the stellar wavefront at both the right and left apertures of the instrument. A novel feedforward algorithm is used to decouple the metrology loop from the left side stellar loop. Experimental results from the testbed are presented that verify this approach and that fully demonstrate the performance of the algorithm.

Keywords: P ointing control, interferometry, FIT, StarLight, formation flying, feedforward, wavefront tilt,

1. INTRODUCTION

The FIT lab is the instrument component testbed of the StarLight Mission technology development program. The StarLight program is charged with developing the necessary technology to enable separated spacecraft interferometry. Spaceborn interferometry holds the promise of realizing astronomical instruments with incredible resolutions that will fundamentally alter our understanding of the Universe.

Interferometry was first used by Albert Michelson in the early 1900's to measure the velocity at which light travels through space. Today we use the interaction of light waves, also called interference, to precisely measure distances and angles. Interferometry is not limited to astrometry, however. Imaging of celestial objects can be achieved by taking multiple measurements of an object at different baselines. To do this requires that the components of the instrument be positioned in a precise formation. In separated spacecraft interferometry instruments with large and adjustable baselines can be realized using multiple spacecraft flying in formation. The large baselines provide effective apertures that cannot be achieved with monolithic space structures, at the cost of introducing relative motion between the component spacecraft of the formation. This relative motion is caused by deadbands in the translational and attitude control systems of the component spacecraft. This relative motion can be compensated for by articulating the optical components of the interferometer. Both optical pathlength[1-3] and stellar wavefront tip/tilt need to be controlled for fringe acquisition. Beam shear in the two directions perpendicular to the line of sight and twist about the line of sight do not need to be controlled for fringe acquisition. This paper focuses on the tip/tilt control system. In the FIT lab this subsystem uses large aperture siderostats and smaller aperture fast steering mirrors (FSM) on both arms, right and left, of the interferometer to control the wavefront tip/tilt. A CCD camera arranged as an angle sensor is used to provide feedback signals.

2. THE FIT POINTING SUBSYSTEM

The layout of the two spacecraft FIT lab is shown in Figure 1. To simulate the relative motion between the component spacecraft the collector optical bench is mounted on a 6 DOF Hexapod (PI M-850). A serial link operating at 100 Hz feeds attitude information from the Hexapod controller to the instrument flight computer. This communication link is meant to mimic the attitude information that would come from a star-tracker/gyro flight configuration. The PI Hexapod is commanded with respect to a fixed inertial coordinate system. This coordinate system is depicted in Figure 1. Three translations in each of the X, Y, and Z directions must be specified as well as three rotations, U, V, and W,abo ut these axes. The U, V,W attitude commands are used to specify the Hexapod attitude in the flight software.

We used the StarLight Mission flight attitude control system (ACS) deadband requirements to prescribe the motion of the Hexapod. In translation, we commanded moves on the order of ± 10.0 millimeters and in rotation we commanded moves on the order of ± 10.0 arc. minutes. The Hexapod controller was programmed with triangular trajectories using a fifth order half range Fourier expansion,

$$\frac{8k_x}{\pi^2}\left(sin((\pi/l_x)\,t) - (1/9)sin((3\pi/l_x)\,t) + (1/25)sin((5\pi/l_x)\,t) - (1/49)sin((7\pi/l_x)\,t) + (1/81)sin((9\pi/l_x)\,t)\right), \quad (1)$$

Joel.F.Shields@jpl.nasa.gov; phone 1 818 354-2376; fax 1 818 393-0342; http://www.jpl.nasa.gov; Jet Propulsion Laboratory, 4800 Oak Grove Drive, Pasadena CA 91109-8099

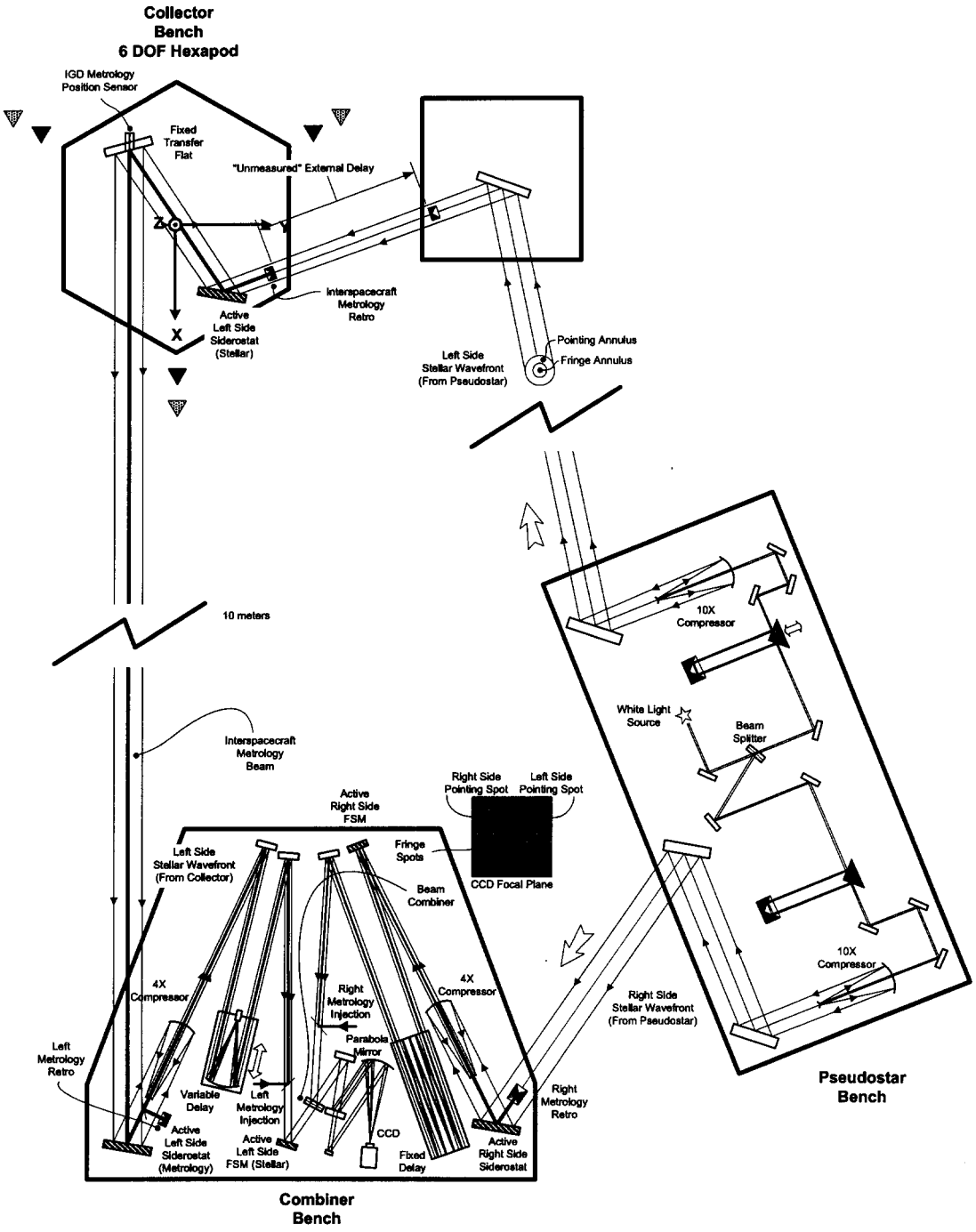

Figure 1. FIT optical benches. The pseudostar bench launches the stellar beam which enters the instrument on the right side at the right combiner siderostat and on the left side at the left collector siderostat. The pointing system is used to align the left and right stellar wavefronts of the instrument. Locations of the active optical components are designated with highlighted elements.

where k_x is the amplitude of the trajectory, in either millimeters or degrees, and l_x is half the triangle wave period. Since the StarLight flight system has a requirement of 30.0 seconds of quiet time between thruster firings, l_x was set to 30.0 seconds. This provided 30.0 seconds of near zero acceleration drift between turn around points of the trajectory.

The combiner bench simulates the component of the instrument aboard the second spacecraft. It is on this bench where light from the left and right sides of the instrument is interfered and the fringe pattern observed. The pseudostar bench is not part of the instrument and serves only to launch the laser source used to imitate the star being observed.

The FIT pointing system is composed of three siderostats and two fast steering mirrors. The locations of each of these active mirrors is shown in Figure 1. Each siderostat (Aerotech AOM130-6M) has an azimuth/elevation gimbal mount actuated in each direction by brushless DC motors (BM75E) driving threaded ball screws. The amplifiers (BAL 20-40-A) are configured in voltage mode to attenuate the effect of ball screw friction. Encoders (4000 line count with quadrature) at the motor armatures are used to close local position loops at a sampling rate of 500 Hz. The bandwidth achieved by these loops was 50 Hz. Each FSM (ThorLabs KC1-PZ) was actuated by three, 8.0 micron stroke, PZT stacks which provide $\pm$36.5 arc. seconds of angular tip/tilt range. The voltages to each of the PZT stacks were controlled in such a way as to eliminate piston motion of the mirror element.[4]

Referring to Figure 1 we can see how feedback signals taken from the CCD camera (Marconi EEV, 40x40 pixels, 24 microns per pixel) and intensity gradient detector (IGD) sensor are used to adjust the three siderostats and two fast steering mirrors in the FIT testbed. Tracing the path of the stellar light on the right side of the instrument, we see that the pseudostar beam is reflected off the large aperture right combiner siderostat before passing through the right side compressor (4x). On the backend of the compressor, the stellar beam is then reflected off the right side fast steering mirror before passing through the fixed delay line (18 meters) and emerging at the second apex mirror. From the second apex mirror the stellar beam is directed toward the beam combiner where light from both sides of the instrument is combined to form an interference fringe. On the right side, the *reflected* light from the beam combiner is split in two annular cross sections, with the outer annulus used as a pointing spot to indicate the position of the fringe spot which is imaged with light from the inner annulus. The two spots are separated spatially and imaged using the CCD at a rate of 100 Hz. On the left side of the instrument, the *transmitted* light from the beam combiner is separated in a similar fashion. In this way, the pointing spots for each side of the interferometer are used as a proxy to stabilize and then interfere the left and right fringe spots. A picture of the CCD image plane is shown in Figure 1. To determine the position of the pointing spots in the focal plane, 9x9 pixel subwindows are wrapped around each image and a simple centroiding algorithm[4] is used to calculate the center of light. It takes approximately two frames, or 20.0 milliseconds, to clock the subwindow pixels out of the image array and pass them to the flight computer.

A description of the two stage (coarse/vernier) two axis (tip/tilt) right side pointing system consisting of the right combiner siderostat, right fast steering mirror and right pointing spot is described in detail in a companion paper.[4] Here we describe the design and performance of the left side stellar loop. This loop is more complex because it is coupled with the left side metrology loop. The metrology loop on the left side is used to maintain an optical link between the two spacecraft as the collector spacecraft moves relative to the combiner spacecraft. This is accomplished by using the left combiner siderostat to point an infrared laser at the IGD located on the collector bench. This sensor provides feedback signals that are used to reposition the left combiner siderostat as the Hexapod is moving. The job of the metrology pointing loop is to null the error of this feedback signal in the presence of Hexapod motion and to acquire the sensor using a "blind" spiral search. A complete description of this loop is given in a second companion paper.[5] Note that as the left combiner siderostat is moved to track the position of the IGD sensor, the incoming stellar light is also perturbed since they share the same optical path. To compensate for this effect, the left collector siderostat must be moved an equal and opposite amount. This is accomplished by feeding forward the encoder measurements from the left combiner siderostat as commands to the left collector siderostat.

In addition, since the Hexapod is free to rotate, this angular motion also impacts the stellar beam by changing the inertial orientation of the collector mirror normals. Since we are assuming that the attitude knowledge of the collector spacecraft is known, this information can also be used as a feedforward signal to the left stellar loop. Similar to the right side, the left side stellar loop uses both a coarse siderostat (collector) and vernier fast steering mirror to position the left side pointing spot. The vernier actuator was an augmentation to the system to increase the pointing accuracy beyond the limitations imposed by the backlash of the siderostat.[4] These actuators are positioned on separate optical benches as can be seen in Figure 1. Note that because of the optical layout, the coupling between the metrology loop and left stellar loop is one way. That is, motion of the left combiner siderostat effects the stellar loop, whereas motion of either the collector siderostat or left side fast steering mirror does not affect the metrology loop.

In the next section of this paper the disturbance environment in the FIT laboratory is characterized. This analysis serves to place an upper limit on the performance that can be achieved, in terms of rms pointing jitter. In section 4 the feedforward pointing control design is presented. Also in this section, the loop shaping of the functionally parallel siderostat and fast steering mirror feedback portion of the controller is described. In section 5 the performance of the pointing system is validated experimentally. In section 6 recommendations are made to improve the disturbance rejection through both active and passive means.

3. POINTING SYSTEM CHARACTERIZATION

In this section we characterize the disturbance environment in the FIT laboratory and use this information to predict the achievable pointing performance. There are several sources of pointing jitter in the FIT lab. At low frequencies, 0-3 Hz, air currents in the lab

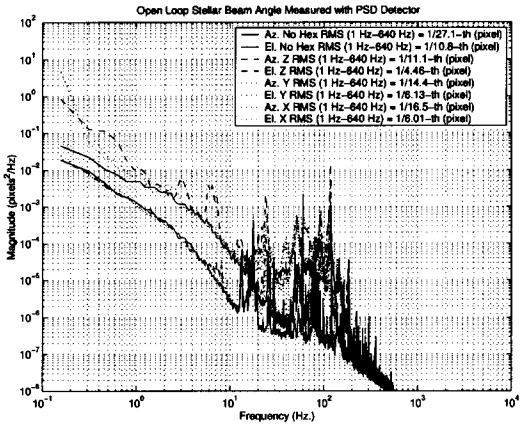

Figure 2. Impact of Hexapod motion on pointing jitter. Cases of no Hexapod motion and translational motion in each of the three Hexapod axes at a rate of 0.33 mm/sec. are shown.

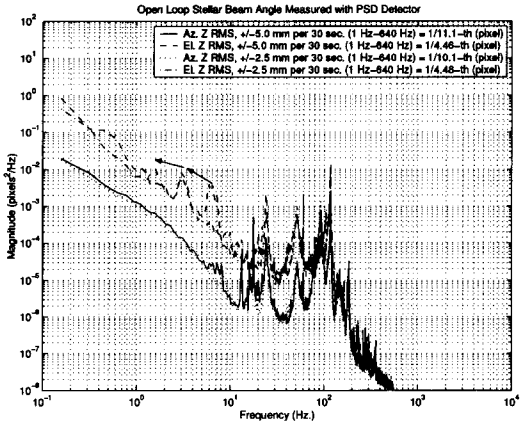

Figure 3. Impact of reducing the Hexapod velocity by a factor of two on pointing jitter. Arrows indicate reduction of the low frequency modes for the two cases.

dominate the rms pointing jitter. These air currents cause slight variations in the density and hence index of refraction of the media through which the stellar light travels. These variations change the incidence angle of the incoming wavefront which is sensed by CCD camera. At higher frequencies, flexible modes of the optical components dominate the pointing jitter. These flexible modes are likely excited by ground vibrations propagating up the legs of the optical benches, which are not isolated with air bearings, and to the optical mounts. The collector bench has an additional source of excitation which is the motor noise generated by the struts of the Hexapod. Each of the six struts are moved using a ball screw powered by brushless DC motors. In addition, we also investigate the possible coupling between delay line motion and pointing jitter. With separated spacecraft interferometry the delay line must slew on the order of 1.0 centimeter to take out optical path length changes caused by low frequency drifts in the spacecraft positions. In the FIT, this motion is achieved using a motor stage to drive the optical components of the delay line. Secondary voice coil and PZT actuated stages provide higher frequency rejection of path length changes.

To characterize these sources of pointing jitter, a position sensing device (OnTrak PSM with OT-301 amplifier) was mounted at the backend of the combiner bench, after the parabola mirror, where it functioned as a two axis angle sensor. This sensor was used as a surrogate for the 100 Hz CCD camera since it could be sampled at a much higher rate and had no delay. A stellar wavefront was launched from the pseudostar and run through the left side of the instrument. Azimuth and elevation pointing data was recorded at a rate of 1.28 kHz with the OnTrak PSD for the case of no Hexapod motion and for three cases of translational Hexapod motion. The Hexapod motion profile used was a 60.0 second period triangle wave with an amplitude of ± 5.0 millimeters. Data was recorded for 250 seconds for each case. Motion in each of the X, Y,and Z directions were tested.

Figure 2 shows the averaged power spectral densities for each of the eight time series (4 cases, each with two axes.). A few important conclusions can be deduced from this data. First, we can integrate the area under these curves to provide us with a time

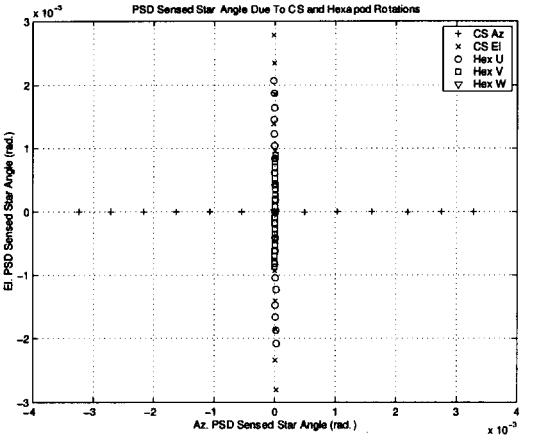

Figure 4. PSD focal plane measurements of stellar beam angle due to rotations of the Hexapod about each of its three inertial axes. U represents rotation about the X axis, V rotation about the Y axis, and W rotation about the Z axis. Also shown is the sensitivity of the focal plane to azimuth and elevation rotations of the collector siderostat gimbal.

domain estimate of the closed loop rms pointing jitter. Using,

$$\sigma = \sqrt{\int_{\omega_1}^{\omega_N} \Phi(\omega) d\omega}, \tag{2}$$

where $\Phi(\omega)$ is the power spectral density, ω_N the Nyquist frequency, and ω_1 an arbitrary starting frequency, the rms pointing error residual with the left stellar closed can be calculated from this open loop data. To do this we choose $\omega_1 = 1.0\,Hz$ since significant disturbance rejection cannot be achieved beyond this frequency due to camera latencies. Figure 2 tabulates these integrals for each of the cases, in terms of 1.0 sigma pixel percentages. Note that without Hexapod motion, the rms jitter for each axis is approximately one half of the jitter with Hexapod translation. So we can conclude that there is a significant high frequency component to the Hexapod motion caused by motor noise. Note also that motion in the Z direction, parallel to the gravity vector, had two modes at 3.0 and 6.0 Hz that did not show up for motion in the X and Y directions, perpendicular to the gravity vector. This is likely due to the larger control effort required to move the payload up and down against gravity as opposed to laterally where the strut velocity is lower.

Figure 3 demonstrates the impact of reducing the velocity of the commanded trajectory from 10.0 mm per 30.0 seconds to 5.0 mm per 30.0 seconds for the case of motion in the Z direction. Note that the two low frequency modes mentioned above are shifted to lower frequencies by one octave. This demonstrates that these modes are related to the spin rate of the motors actuating the struts, possibly due to periodic eccentricities in the ballscrew mechanism. Note also that the rms errors for both speeds are about the same indicating that reducing the velocity of the Hexapod trajectory will not proportionately reduce the observed jitter.

Note that in both Figures 2 and 3 the elevation jitter was larger then the azimuth jitter. This is because the bending modes of the optical mounts are more susceptible to vibrations then the torsional modes. Since only the torsional modes would change beam angles in the azimuth direction, jitters in this direction are smaller than in the elevation direction.

Similar PSD experiments were completed to characterize pointing jitter caused by delay line motion. For slewing of both the delay line motor and voice coil stages no increase in the PSD jitter was observed. Displacement of the PZT stage was found to impact stellar beam angle in the azimuth direction. This, however,w as not caused by flexible coupling between the delay line and PSD sensor. This effect was due to defocus of the delay line catseye with piston motion of the PZT mirror. This is a deterministic effect that can be compensated for using measurements of the voltage commands to the PZT.

3.1. Collector Optical Sensitivity

In addition to the dynamic characterization of the Hexapod, for control system design and simulation we also require the sensitivity between the Hexapod rotations and stellar beam angles. Since rotations of the Hexapod can change the direction of the stellar beam as it passes through the collector optics, this effect must be compensated for by moving the collector siderostat in an appropriate way. This sensitivity can be determined analytically using orientation knowledge of the collector siderostat and transfer mirror. Alternatively, we can experimentally determine this sensitivity by rotating the Hexapod in each of its three degrees of freedom and measure the azimuth and elevation angle changes of the stellar beam at the combiner,befo re the left compressor. Figure 4 shows these angle measurements for 20 positions about each degree of freedom within the expected ± 10.0 arc. min. range of motion of the Hexapod. Note that for rotations about the vertical axis of the Hexapod, W,no change in the beam angle was observed. This is because the mirror normals of the collector siderostat and transfer mirror are rotated about the same axis by the same amount, causing the optical arrangement to act

as a retro reflector about this axis. Rotations of the Hexapod about either of the cross axes, U or V, rotate the two mirror normals by a different amount causing a net change in the orientation of the stellar beam. This change is only in the elevation axis, however, since the projection of any rotation vector onto the azimuth axis of the siderostat and transfer flat is equal. This is because the azimuth axes of these two mirrors are collinear. The elevation changes because these axes are different and the projection of the rotation vector onto these two axes is unique.

The equal spacing of the plot symbols in Figure 4 suggest that the sensitivity can be modelled as a linear relationship between the U, V, W rotations and azimuth and elevation beam angles. In terms of a linear input/output relationship, the sensitivity was determined to be,

$$\mathbf{T}_{UVW}^{Az.El.} = \begin{bmatrix} -0.005717 & -0.001525 & 0.000205 \\ 0.713366 & -0.301692 & 0.000635 \end{bmatrix} \tag{3}$$

where the input and output angles are in units of radians. This sensitivity can be expected to change depending upon the specific orientation of the collector siderostat.

4. FEEDFORWARD CONTROLLER DESIGN

Figure 5 provides a detailed block diagram of the left side pointing system including a model of how Hexapod translations and rotations disturb the left stellar loop. As the metrology loop responds to track the motion of the IGD sensor, the stellar beam is perturbed by the motion of the left combiner siderostat mirror. This disturbance is shown in Figure 5 as entering the left stellar loop between the gains $1/r_{arm}$ and k_{beam}. As described in the previous section, rotations of the Hexapod also perturb the stellar beam. This disturbance is shown in Figure 5 just after the metrology loop disturbance. Additionally, the high frequency jitters are modelled as colored measurement disturbances. White pixel noise, $v_{x_{ccd}}^{pixel}$ and $v_{y_{ccd}}^{pixel}$, also corrupts the CCD measurements before they are sampled and used as feedback. To simulate the jitter environment in the FIT, the high rate PSD data was sub-sampled at 100 Hz and imported directly to the simulation. This avoided the necessity of modelling the plethora of modes in Figure 2 between 10 Hz and 100 Hz for design of a shaping filter.

To compensate for the effect of the rigid body Hexapod motion on the left stellar loop, measurements of the combiner siderostat encoders and Hexapod attitude telemetry are used as feedforward signals. The Hexapod attitude data is converted to azimuth and elevation stellar beam angles in sky coordinates by using an estimate of the true collector optical sensitivity, $\mathbf{T}_{UVW}^{Az.El.}$, $\hat{\mathbf{T}}_{UVW}^{Az.El.}$. These signals are then mapped to encoder space using the gains GR and $1/k_{beam}$ and added with the azimuth and elevation left combiner siderostat encoder measurements. The total feedforward signal is then partitioned as additive tip/tilt commands to both the FSM and collector siderostat. The compensators $C_{Az./El.}^{SD\,FF}$ and $C_{Az./El.}^{FSM\,FF}$ are shaped in the frequency domain to pass DC and low frequency (1.5 Hz) signal components to the siderostat and high frequency components to the FSM. Additionally,th e command passed on to the FSM is multiplied by $k_{FF} = (1/GR) \cdot k_{comp}$ to transform the commands from siderostat encoder coordinates to FSM tip/tilt angles. Nominally the frequency components of the feedforward signal are low so the gain, k_{FF}^{tune},w as included to null this command path by setting it to zero.

A number of error sources exist in the feedforward information that potentially deteriorate its effectiveness. These sources deserve mention because they may help elucidate the operation of the system. None of these error sources are functionally significant. The most obvious discrepancy comes from the time delays associated with the local collector siderostat encoder loop. Because of these delays, the feedforward command is not instantaneously applied. The bandwidth of this loop is, however, an order of magnitude faster than the camera feedback path (50 Hz verse ~5.0 Hz). Backlash at the combiner siderostat also causes a knowledge uncertainty in the feedforward signals since the encoder measurements used to estimate the mirror tip and tilt are incorrect by the state of the backlash. In addition, backlash at the combiner siderostat causes a discrepancy between the commanded correction and the achieved correction. Neither of these backlash effects are large compared to the total excursion of the siderostats during tracking. The Hexapod telemetry can also be in error because of the communication delays in the serial link between the Hexapod processor and the instrument processor. The consequence of these delays are that the available commands represent the attitude commands from some time ago. These latencies should be kept a small percentage of the telemetry rate. Furthermore, the attitude telemetry represents the command sent to the Hexapod controller not the measured attitude, so some small transient errors will exist between the commanded and true attitude.

4.1. Feedback Design

In most feedback controller designs, the sampling rate imposes a fundamental limitation on the achievable bandwidth. A general rule of thumb used by control system designers is that the bandwidth of the closed loop system will be one decade lower then the sample rate. In this application, we are futher restricted by the latencies of the feedback sensor. These latencies are modelled by a pure time delay of two frames, T_{fd}= 0.02 $(sec.)$, in Figure 5. Because of this time delay, the bandwidth achieved with acceptable phase and gain margins using the 100 Hz camera was approximately 7.0 Hz. Figure 6 shows the open loop bode plots for the siderostat path, the FSM path, and the parallel connection of the two. Note the severe degradation of the phase at about 10.0 Hz due to the time delays.

The loop shapes for each actuator have been designed to maximize dynamic range and disturbance rejection of the pointing system. At low frequency, the siderostat is given a much larger gain than the FSM and a slope of two integrators. The double integrator provides

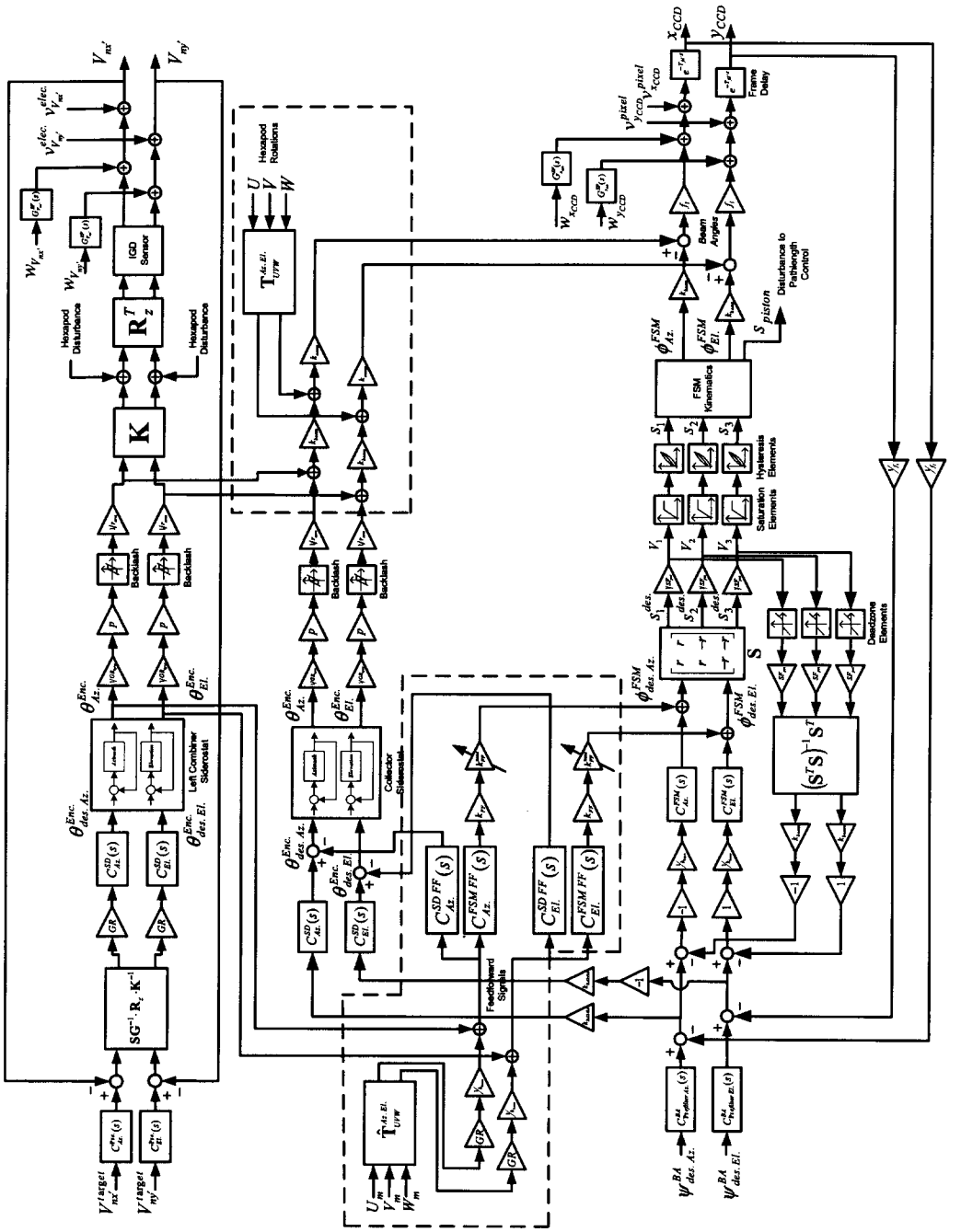

Figure 5. Left side FIT pointing system. Left combiner siderostat encoder and Hexapod attitude information are used as feedforward signals to the left stellar loop. Camera pointing spot centroids are used for feedback. Dotted areas indicate feedforward components discussed in this paper. The other components are mentioned in the text and discussed in more detail in two companion papers.

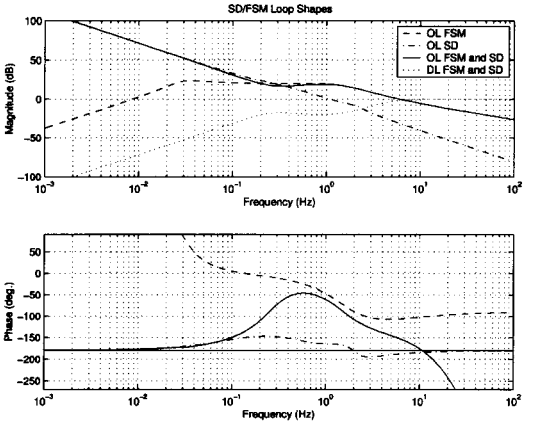

Figure 6. Left stellar loop siderostat and FSM loop shapes. Parallel connection of the two actuators and disturbance rejection achieved are also shown.

the siderostat feedback path with the ability to reject ramp type disturbances caused by attitude and formation control deadbands. Since the siderostat has a much higher gain at low frequency, the FSM range of motion is not used to compensate these larger low frequency errors. At high frequency, the FSM has a higher gain and is used to correct for a relatively larger portion of the smaller high frequency errors. The siderostat and FSM loop shapes, intersection frequency, and crossover locations in Figure 6 are designed to prevent saturation of the FSM. Additionally, the beam angle commands to the loop are prefiltered to keep the error signals in the loop small when a change in the pointing spot location is requested. If disturbances are large enough, however,sa turation of the FSM is possible. To prevent instability in this regime, an additional feedback of the PZT voltages (See Figure 5.) is included to increase dissipation during a saturation event.

5. SIMULATION AND TESTBED EXPERIMENTS

The pointing system shown in Figure 5 was coded in a Matlab/Simulink environment to facilitate algorithm development. We used disturbance data for motion of the Hexapod in the Z direction at a rate of 0.33 mm per second, since this represented the worst case jitter environment. The Simulink model does, however, have the capability of simulating full 6 DOF Hexapod motion with arbitrary trajectories for validation of the feedforward component. The simulation demonstrated rms pointing errors of 1/8.84-th of pixel in azimuth and 1/4.23-th of pixel in elevation, numbers very similar (1/11.1-th and 1/4.46-th) to the predicted performance given in the Section 3 for this case of Hexapod motion. The simulation numbers are a bit better because of the small amount of extra disturbance rejection between 1.0 and 10.0 Hz not accounted for by the rms integrals (See Figure 6.). Cases of step changes in the commanded beam angle were also tested, prior to implementation, to confirm proper coordination between the coarse siderostat motion and FSM motion.

The experimental tracking performance of the left side FIT pointing system is shown in Figure 7. From left to right this experiment shows three phases of operation. Initially, the stellar spot is acquired in the subwindow and the centroiding algorithm is providing measurements of the star position with respect to a local coordinate frame centered in the subwindow. At t = 30.0 seconds a command is sent to close the pointing loop using both feedforward and feedback signals. This takes out the bias in the centroid measurements and regulates the spot position about the origin of the local coordinate frame. At t = 75.0 seconds commands are sent to begin motion of the Hexapod. The Hexapod was commanded to move by ± 10.0 millimeters in the X, Y and Z directions, and by ± 10.0 arc. minutes in rotations about these axes, following the trajectory defined by Equation (1). Note the increase in pointing jitter, particularly in the elevation axis, at the onset of Hexapod motion, but that the error signal has zero bias in spite of the large Hexapod motion that would otherwise throw the star image off the focal plane of the camera.

Figure 8 is included as a validation of the feedforward component of the control system. In this experiment the feedback from the camera is disabled by multiplying the error signal by zero. This leaves only the feedforward signals active. The Hexapod was commanded to move a small amount, enough to see its impact on the spot position but not enough to throw the spot off the subwindow. This allowed data logging of the spot position since the image remained in the centroiding subwindow. At t = 65.0 seconds the feedforward is turned on and the low frequency variation of the spot position caused by Hexapod motion is eliminated demonstrating the efficacy of the feedforward information.

6. CONCLUSIONS/RECOMMENDATIONS

We have seen that the achievable performance of the left side pointing system is limited by high frequency flexible modes associated with motion of the Hexapod. These modes prevent achieving the 1/10-th of a pixel requirement set out in the flight interferometer

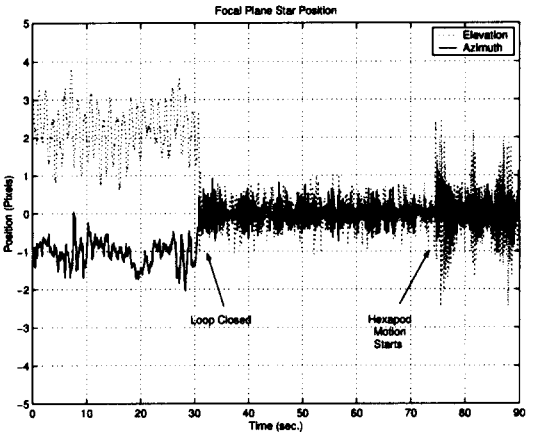

Figure 7. Experimental left side star position. The first event denoted in the figure is locking on the star position with a commanded beam angle of (0.0,0.0). The second event is the onset of hexapod motion.

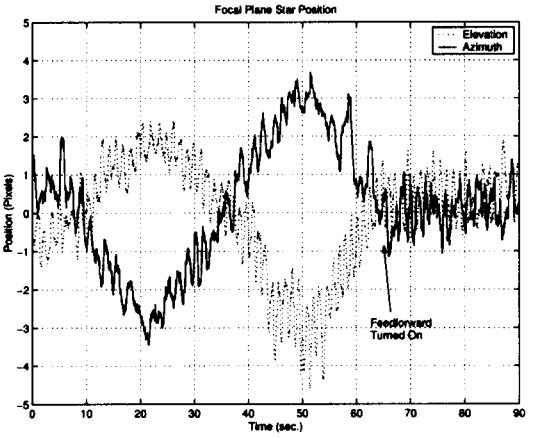

Figure 8: Experimental left side star position using only feedforward signals to cancel the effect of hexapod motion.

performance model (IPM).[6] By itself increasing the sampling rate of the camera to 200 Hz is not likely to increase disturbance rejection enough to meet the jitter requirement. Calculations of rms jitter using Equation (2) for motion of the Hexapod in the Z direction showed that the elevation jitter went from 1/4.46-th of a pixel to 1/4.7-th of a pixel when the integral was summed from 2.0 Hz instead of 1.0 Hz. Adding accelerometers to the collector bench and using these signals to cancel the Hexapod jitters could conceivably reduce the jitter to the case of no Hexapod motion, or 1/10.8-th of a pixel. This would meet the pointing requirement, but there are questions as to sensor placement and development time to integrate these acceleration feedforward signals with the existing pointing system.

Passive means of noise cancellation offers a faster and cheaper alternative. If the combiner bench were floated with isolated legs, the best we could expect to see is that the elevation jitter improves to what we see in the azimuth axis. If we take this amount of jitter (1/27.1-th pixel) and add the increase that we see in the elevation axis when the hexapod moves (1/7.6-th of a pixel) we can expect to see 1/6.0-th of a pixel of remaining jitter, an improvement of 1/17.0-th of a pixel. This combined with active means of cancellation offers the hope of surpassing the jitter requirement.

A better method of introducing relative motion between the optical benches would be to use a voice coil actuated hexapod instead of DC motors. Voice coils provide a smooth non-contact linear displacement mechanism that is more appropriate for interferometry applications. The drawback of using voice coils is that they provide much less force then a geared DC motor, but this limitation could be overcome by offloading the payload with a counter weight.

ACKNOWLEDGMENTS

The authors wish to thank the support of Gary Blackwood. The research described in this paper was carried out at the Jet Propulsion Laboratory, California Institute of Technology, under a contract with the National Aeronautics and Space Administration.

REFERENCES

1. J. J. Hench, B. J. Lurie, R. Grogan, and R. Johnson, "Implementation of Nonlinear Control Laws for the RICST Optical Delay Line," IEEE Aerospace Conference, IEEE, (Big Sky,Mo ntana), March 2000.
2. B. J. Lurie and P.J. Enright, *Classical Feedback Control With MATLAB*,Marc el Dekker Inc., New York, 2000.
3. B. J. Lurie, J. J. Hench, A. Ahmed, and F. Y. Hadaegh, "Nonlinear Control of the Optical Delay Line Pathlength," **3692**, pp. 139–149, SPIE, (Orlando, Florida), April 1999.
4. J. Shields, S. Sirlin, and M. Wette, "Starlight Pointing Subsystem for the Formation Interferometer Testbed (FIT),"IEEE Aerospace Conference, IEEE, (Big Sky,Mo ntana), March 2002.
5. J. Shields, S. Sirlin, and M. Wette, "Metrology Sensor Characterization and Pointing Control for the Formation Interferometer Testbed (FIT)," IEEE Aerospace Conference, IEEE, (Big Sky, Montana), March 2002.
6. O. Lay, "Starlight Interferometer Performance Model D-20707," Internal Document, Jet Propulsion Laboratory,Ja nuary 2002.
7. M. Born and E. Wolf, *Principles of Optics*,Cam bridge University Press, 1999.
8. R. M. Murray, Z. Li, and S. S. Sastry,*A Mathematical Introduction to Robotic Manipulation*,CRC Press, 1994.
9. J. J. E. Slotine and W. Li, *Applied Nonlinear Control*,Prentice-H all, 1991.
10. G. W. Neat, J. W. Melody, and B. J. Lurie, "Vibration Attenuation Approach for Spaceborne Optical Interferometers," *IEEE Transactions on Control Systems Technology* **6**, pp. 689–700, November 1998.